



**HAL**  
open science

## **An innovative GC-MS, NMR and ESR combined, gas-phase investigation during chemical vapor deposition of silicon oxynitrides films from tris(dimethylsilyl)amine**

Laura Decosterd, Konstantina Christina Topka, Babacar Diallo, Diane Samelor, Hugues Vergnes, François Senocq, Brigitte Caussat, Constantin Vahlas, Marie-Joëlle Menu

### **► To cite this version:**

Laura Decosterd, Konstantina Christina Topka, Babacar Diallo, Diane Samelor, Hugues Vergnes, et al.. An innovative GC-MS, NMR and ESR combined, gas-phase investigation during chemical vapor deposition of silicon oxynitrides films from tris(dimethylsilyl)amine. *Physical Chemistry Chemical Physics*, 2021, 23 (17), pp.10560-10572. 10.1039/d1cp01129d . hal-03220403

**HAL Id: hal-03220403**

**<https://hal.science/hal-03220403>**

Submitted on 7 May 2021

**HAL** is a multi-disciplinary open access archive for the deposit and dissemination of scientific research documents, whether they are published or not. The documents may come from teaching and research institutions in France or abroad, or from public or private research centers.

L'archive ouverte pluridisciplinaire **HAL**, est destinée au dépôt et à la diffusion de documents scientifiques de niveau recherche, publiés ou non, émanant des établissements d'enseignement et de recherche français ou étrangers, des laboratoires publics ou privés.

**An innovative GC-MS, NMR and ESR combined, gas-phase investigation during chemical vapor deposition of silicon oxynitrides films from tris(dimethylsilyl)amine**

*Laura Decosterd, Konstantina Christina Topka, Babacar Diallo, Diane Samelor, Hugues Vergnes, François Senocq, Brigitte Caussat, Constantin Vahlas, Marie-Joëlle Menu\**

Laura Decosterd, Prof. Marie-Joëlle Menu\*  
CIRIMAT, Université de Toulouse, CNRS, Université Toulouse 3 - Paul Sabatier,  
118 Route de Narbonne,  
31062 Toulouse cedex 9 – France  
menu@chimie.ups-tlse.fr

Diane Samelor, Konstantina. C. Topka, Dr. François Senocq, Dr. Constantin Vahlas  
CIRIMAT, Université de Toulouse, CNRS, INP- ENSIACET  
4, allée Emile Monso, BP-44362,  
31030 Toulouse Cedex 4, France

Konstantina. C. Topka, Dr. Hugues Vergnes, Prof. Brigitte Caussat  
LGC, Université de Toulouse, CNRS, INP- ENSIACET  
4, allée Emile Monso, BP-44362,  
31030 Toulouse Cedex 4, France

Dr. Babacar Diallo, CNRS, Conditions Extrêmes et Matériaux : Haute Température et Irradiation (CEMHTI) UPR 3079, Université d'Orléans,  
Site Cyclotron, CS 30058  
3A rue de la Férolierie  
45071 Orléans cedex 2, France

Keywords: Silicon oxynitride, TDMSA, thermal CVD, GC-MS, ESR, NMR, gas phase analysis

## Abstract

Tris(dimethylsilyl)amine (TDMSA) is used in the presence of O<sub>2</sub> and NH<sub>3</sub> for the atmospheric pressure chemical vapor deposition (CVD) of conformal, corrosion barrier silicon oxynitride (SiO<sub>x</sub>N<sub>y</sub>) films at moderate temperature. Plausible decomposition pathways taking place during the process, as well as resulting gas-phase by-products, are investigated by an innovative methodology, coupling solid-state films characteristics with gas phase analysis. Liquid NMR, gas chromatography coupled with mass spectrometry (GC-MS) and electron spin resonance (ESR) allow probing stable compounds and radical intermediate species in the gas phase. At least fifteen by-products are identified, including silanols, siloxanes, disilazanes, silanamines, and mixed siloxane-silanamine molecules, in addition to more usual compounds such as water. The radical dimethylsilane, Me<sub>2</sub>HSi<sup>•</sup>, is noted across all experiments, hinting at the decomposition of the TDMSA precursor. Deposition of SiO<sub>x</sub>N<sub>y</sub> films occurs even in absence of NH<sub>3</sub>, demonstrating the judicious choice of the silanamine TDMSA as a dual source of nitrogen and silicon. Additionally, the presence of Si-H bonds in the precursor structure allows formation of SiO<sub>x</sub>N<sub>y</sub> films at temperatures lower than those required by other conventional silazane/silanamine precursors. Addition of NH<sub>3</sub> in the inlet gas supply results in lower carbon impurities in the films. The identified by-products and formulated decomposition and gas-phase reactions provide stimulating insight and understanding of the deposition mechanism of SiO<sub>x</sub>N<sub>y</sub> films by CVD, offering possibilities for the investigation of representative chemical models and process simulation.

## 1. Introduction

Silicon oxynitride ( $\text{SiO}_x\text{N}_y$ ) films attract a lot of attention<sup>1</sup> due to their remarkable intrinsic and tunable properties, which are in-between those of silica ( $\text{SiO}_2$ ) and silicon nitride ( $\text{Si}_3\text{N}_4$ ) films. The atomic network of amorphous  $\text{SiO}_x\text{N}_y$  is denser than that of  $\text{SiO}_2$  due to the partial replacement of O anions by highly coordinated N ones and for this reason such films present better thermal and chemical stability,<sup>2</sup> superior hardness<sup>3</sup> and enhanced anti-corrosion properties.<sup>4</sup> At the same time, a  $\text{SiO}_x\text{N}_y$  material presents reduced intrinsic mechanical stress, which commonly describes the more rigid  $\text{Si}_3\text{N}_4$ , avoiding thus the emergence of cracks that can be detrimental to product performance.<sup>5,6</sup> Even at nitrogen concentrations as low as 10 at.%,  $\text{SiO}_x\text{N}_y$  films have been reported to reduce buffered HF etching rate and  $\text{Na}^+$  diffusion.<sup>7</sup> Due to these properties, silicon oxynitride films and coatings gathered interest for applications in the fields of solar cells,<sup>8,9</sup> semi-conductors<sup>10,11</sup> and packaging.<sup>2</sup>

$\text{SiO}_x\text{N}_y$  films have been deposited by different techniques, however, when dealing with uniform, conformal and micrometer thick films deposited on thermally sensitive and complex substrates with non-line-of-sight geometries, chemical vapor deposition (CVD) is one of the most suitable methods.<sup>12</sup> Silane ( $\text{SiH}_4$ ) or chlorosilanes are often involved as the silicon-providing precursors and are introduced in the CVD process along with oxidants such as  $\text{N}_2\text{O}$ ,  $\text{NO}_2$  or  $\text{O}_2$ , with ammonia ( $\text{NH}_3$ ) being conventionally used as the nitrogen source. Nonetheless, in thermal CVD processes, which lack plasma activation, temperatures higher than  $750^\circ\text{C}$  are required to obtain oxynitride films.<sup>13</sup> As such, it becomes evident that the choice of precursor and the inlet gas composition are the key factors that enable thermal CVD of  $\text{SiO}_x\text{N}_y$  films in lower desired temperature windows.

In that context, the presence of Si-H bonds in the precursor is essential for the reduction of the deposition temperature, as these bonds are known to be easily oxidized and have been reported to activate the deposition mechanism and promote film formation.<sup>14</sup> As an example, the case of hexamethyldisilazane ((CH<sub>3</sub>)<sub>3</sub>SiNHSi(CH<sub>3</sub>)<sub>3</sub>, HMDSz) is noted, a molecule which does not contain Si-H bonds, and for which the lowest reported temperature for deposition of SiN<sub>x</sub> or SiO<sub>x</sub>N<sub>y</sub> films by thermal CVD is 760°C.<sup>13</sup> Contrary to HMDSz, upon addition of Si-H bonds in the precursor molecule, deposition temperatures can be effectively decreased, as illustrated through the bis(tertiary-butylamino)silane (BTBAS) precursor, which contains two Si-H bonds and allows the deposition of SiN<sub>x</sub> at 600-675°C,<sup>15</sup> with temperatures down to 550°C also being reported.<sup>16</sup> The presence of additional Si-H bonds is thus expected to decrease the minimum deposition temperature even further.

Other important information that needs to be taken into account during selection of suitable precursor molecules for SiO<sub>x</sub>N<sub>y</sub> deposition by thermal CVD is the presence of Si-O bonds. Such bonds can impede the incorporation of nitrogen, as reported by Park et al.,<sup>17</sup> who studied the deposition of SiO<sub>2</sub> from 3-aminopropylmethyldiethoxysilane (APMDES) at 650°C by thermal CVD. The authors noted that no nitrogen was detected in the films despite the high temperature. In the same sense, Vamvakas et al.<sup>18</sup> performed thermodynamic calculations for the thermal CVD of SiO<sub>x</sub>N<sub>y</sub> from tetraethoxysilane (TEOS) mixtures, concluding that incorporation of nitrogen is not possible at temperatures below 930°C or 830°C, in the presence of N<sub>2</sub>O or NH<sub>3</sub> gas, respectively, the biggest hindrance being the four oxygen atoms surrounding the Si atom in the precursor molecule. It is therefore suggested that the presence of Si-O bonds is unfavorable when the production of a SiN<sub>x</sub> or SiO<sub>x</sub>N<sub>y</sub> film is desired at moderately low temperatures, and by contrast, a Si-N bond in the starting precursor should be favored. Although the vast majority of thermal CVD

processes utilize  $\text{NH}_3$  as a nitrogen source, the innate presence of nitrogen in the precursor itself could prove beneficial when high nitrogen contents are targeted.

In light of the above, the present work focuses on the decomposition mechanisms of tris(dimethylsilyl)amine ( $\text{N}(\text{SiHMe}_2)_3$ , TDMSA) that is being used by the authors as precursor in the CVD of  $\text{SiO}_x\text{N}_y$  films. TDMSA is selected given the presence of the desired Si-N and Si-H bonds, while avoiding Si-O ones. Compared to conventional precursors used in CVD of  $\text{Si}_3\text{N}_4$  and  $\text{SiO}_x\text{N}_y$ , such as silane ( $\text{SiH}_4$ )<sup>7, 8</sup> and dimethyldichlorosilane ( $\text{SiCl}_2(\text{CH}_3)_2$ ),<sup>19, 20</sup> it presents lower handling risks and by-passes the production of ammonium chloride encountered during deposition using chlorosilanes. However, it is a complex molecule with a large number of bonds; the silicon atoms are involved in a tertiary amine, from which many plausible decomposition pathways and products are expected. Therefore, gaining insight into the deposition mechanism and understanding the CVD process from this new precursor requires detailed analysis of both the solid and the gas phase.

Gas phase analysis methods implemented in CVD processes is a common, though not trivial tool to access the deposition mechanisms. For example, in situ UV spectroscopic or FTIR exhaust gas studies have been used to establish chemical reactions paths in the CVD of gallium nitride (GaN) films,<sup>21, 22</sup> and gas chromatography coupled with mass-spectrometry (GC-MS) was applied to investigate the thermal decomposition and by-products generation in CVD of titanium nitride (TiN) films.<sup>23</sup> More recent implementations involve in situ Raman spectroscopy during thermal decomposition of a tungsten imido complex by aerosol-assisted (AA)CVD,<sup>24</sup> or in situ optical emission spectroscopy during microwave plasma-enhanced chemical vapor deposition of phosphorus (P) and nitrogen (N) co-doped nanocrystalline diamond.<sup>25</sup> Focusing on analogous studies of CVD processes involving silicon-containing precursors, the majority of the reported

literature concerns the binary systems SiC, SiO<sub>2</sub> or Si<sub>3</sub>N<sub>4</sub> from chlorosilanes, silanes or TEOS. Among them, Zhang et al.<sup>26</sup> used GC-MS for the characterization of the gas phase during the deposition of SiC from methyltrichlorosilane in the presence of H<sub>2</sub>, identifying HCl and SiCl<sub>4</sub> molecules as by-products. In the same context, Arno et al.<sup>27</sup> used online FT-IR analysis, detecting primarily carboxylic acids and water, among other compounds, during the SiO<sub>2</sub> deposition from TEOS and O<sub>3</sub>. As for Si<sub>3</sub>N<sub>4</sub> films, the gas phase characterization and deposition mechanisms from SiH<sub>4</sub> and NH<sub>3</sub> by photo-assisted CVD, or from SiH<sub>2</sub>Cl<sub>2</sub> and NH<sub>3</sub> by low-pressure CVD have been investigated by transient mass spectroscopy.<sup>28, 29</sup>

Despite the existing literature for these chemical systems and materials, the gas phase characterization of a ternary SiO<sub>x</sub>N<sub>y</sub> and a fortiori quaternary SiO<sub>x</sub>N<sub>y</sub>C<sub>z</sub> system remains rather unexplored. In this context, Fainer et al. investigated gas mixtures of 1,1,3,3-tetramethyldisilazane (HSi(CH<sub>3</sub>)<sub>2</sub>)<sub>2</sub>NH (TMDS) with O<sub>2</sub> and N<sub>2</sub> during plasma chemical decomposition for SiC<sub>x</sub>N<sub>y</sub>O<sub>z</sub>:H nanocomposite films.<sup>30</sup> Their gas phase characterization by in situ optical emission spectroscopy revealed potential formation of volatile products such as methane CH<sub>4</sub> and CO. However, silicon-containing compounds were absent from their study. More generally, the majority of publications on the CVD of SiO<sub>x</sub>N<sub>y</sub> films focus mostly on their solid phase characterization and report the gas phase inadequately. However, control and consequently modeling, simulation and ultimately optimization of these complex-in-chemistry processes require comprehensive insight in the gas and surface chemistries.<sup>31</sup> For this reason, a coupled solid and gas phase analysis proves to be useful in determining potential starting precursors and experimental conditions for the formation of functional films at the lowest possible deposition temperature, as well as in formulating kinetic models for eventual process optimization through utilization of computational fluid dynamics simulations.

Given all that has been presented so far, the present work focuses on the gas phase characterization of a TDMSA-O<sub>2</sub>-NH<sub>3</sub> and TDMSA-O<sub>2</sub> CVD process operating at atmospheric pressure, by simultaneously combining classical, multiple physico-chemical methods used in molecular chemistry. A new methodology is proposed, involving gas chromatography coupled with mass spectrometry (GC-MS), nuclear magnetic resonance (NMR) and electron spin resonance (ESR) for the analysis of the gaseous effluents. In particular, ESR, commonly applied for the molecular structural characterization of paramagnetic species, can be used for the characterization of the gas phase,<sup>32</sup> constituting an innovative approach for the identification of radical species in CVD processes. Thus, the combination of these three analytical techniques enables the identification of the by-products and intermediates involved in the deposition process.

First, we investigate the thermal behavior of the TDMSA precursor in order to determine its lowest decomposition temperature and the chemical nature of the produced by-products. Then, we undertake deposition experiments with and without ammonia in order to identify the origin of the nitrogen atoms incorporated in the SiO<sub>x</sub>N<sub>y</sub> films. This parallel investigation of the gas phase alongside the compositional characterization of the deposited thin films by ion beam analysis (IBA) helps in correlating potential changes in the solid phase to the different by-products identified in the gas phase. This simultaneous consideration, for a set of diverse process parameters (temperature, oxygen and ammonia flow rates), and the thickness and composition of the deposited SiO<sub>x</sub>N<sub>y</sub> films allows proposing a plausible deposition mechanism, which could be utilized for the development of apparent chemical models and simulation.

## **2. Experimental Section**



## 2.1. Materials

Tris(dimethylsilyl)amine ( $\text{N}(\text{SiHMe}_2)_3$ , TDMSA, **14**), 1,1,3,3-tetramethyldisiloxane ( $\text{O}(\text{SiHMe}_2)_2$ , TMDSO, **3**), pentamethyldisiloxane ( $\text{O}(\text{SiHMe}_2)(\text{SiMe}_3)$ , PMDSO, **6**), 1,1,3,3,5,5-hexamethyltrisiloxane ( $\text{Me}_2\text{Si}(\text{OSiHMe}_2)_2$ , HMTSO, **11**), 1,1,3,3-tetramethyldisilazane ( $\text{HN}(\text{SiHMe}_2)_2$ , TDMSz, **7**), methoxytrimethylsilane ( $\text{MeOSiMe}_3$ , MeOTMS, **2**) were purchased from ABCR. Trimethylsilanol ( $\text{Me}_3\text{SiOH}$ , **4**), hexamethyltricyclosiloxane ( $(\text{Me}_2\text{SiO})_3$ , HMCTSO, **12**), potassium bromide (KBr, FT-IR grade),  $\alpha$ -(4-pyridyl-1-oxide)-N-tert-butylnitron ( $\text{C}_{10}\text{H}_{14}\text{N}_2\text{O}_2$ , POBN), hexamethyldisilazane ( $\text{HN}(\text{SiMe}_3)_2$ , HMDSz, **10**), dimethylsulfoxide- $\text{d}_6$  (DMSO- $\text{d}_6$ ) and toluene were purchased from Sigma-Aldrich. All the products are used as received.

## 2.2. Silicon oxynitride deposition

The experimental setup has already been presented in previous work.<sup>33</sup> The exit of the reactor setup was slightly modified as illustrated in Figure S1 of *Supporting Information*, to enable the sampling for the three gas phase analyses. Silicon  $\langle 100 \rangle$  wafers (Neyco,  $24 \times 32 \text{ mm}^2$ ) are used as substrates. Before being inserted into the reactor, they were degreased in a succession of three ultrasound bath steps, including: 1) an ultrasound bath using distilled water for 5 min, then rinsed with acetone, 2) an ultrasound bath using acetone (>99%, VWR Chemicals) for 5 min, then rinsed with ethanol, 3) an ultrasound bath using ethanol (99.3%, VWR Chemicals) for 5 min, and finally dried under Ar (99.9999%, Messer) flow. Within the reactor, the substrates were supported vertically by home-made, tubular, stainless steel substrate holders, with a 7 mm deep insertion slot, positioned on the row. Their total length was 450 mm, supporting a maximum of 18 coupons for each run. Across all experiments utilizing various operating conditions, the coupon positioned at 380 mm from the inlet is systematically used to extract information on the average deposition rate

and composition in nitrogen and carbon, and compare the values obtained from different experiments.

### 2.3. Characterizations of the gas phase and of the film composition

Sampling for GC-MS analysis of the gas phase is done using a 1L Tedlar push lock valve PLV sampling bag with Thermogreen LB-2 Septa (Sigma-Aldrich). Analysis is performed with a Trace 1310 gas chromatograph coupled with a TSQ 900 (Agilent Technologies) mass spectrometer (MS), equipped with a TG-5SILMS column (Thermo Scientific, 30 m length, 0.25 mm id, 0.25  $\mu\text{m}$  film thickness). Helium is used as carrier gas with split mode injector, inserted at 250°C with a flow rate programmed at 1 mL min<sup>-1</sup> for 12 min, then increased and held at 3 mL min<sup>-1</sup> for 8 min. Column temperature is programmed held at 25°C for 10 min, then increased to 140°C with a 23°C.min<sup>-1</sup> ramp, and finally maintained at 140°C for 5 min. For every analysis, the transfer line to the MS ion source is set to 250°C and the MS is used in scan mode with a range from 10 to 600 amu. Using this method, the commercially available silane-based by-products are analyzed in order to corroborate assignments. External calibration is applied for TDMSA with the aim to provide decomposition/conversion percentages. For this purpose, four Tedlar bags are filled with TDMSA and N<sub>2</sub> at room temperature, by flowing 0.8, 1.13, 1.4 and 2 standard cubic centimeters per minute (sccm) of TDMSA through the reactor. Each bag is analyzed 3 times and, for each TDMSA flow rate, the mean surface area of TDMSA is normalized to the N<sub>2</sub> surface area. The derived calibration curve is confirmed by using additional bags filled with 1.7 and 1.55 sccm of TDMSA, and comparing the calculated to the experimental values, out of which an error margin of 11 % is established. Calibration curve is given in Figure S2 of *Supporting Information*.

The NMR analysis of TDMSA precursor is performed in DMSO- $d_6$  as a solvent on a Bruker Avance II operating at 400 MHz equipped with a TBO probe. For the NMR analysis of the gas phase during deposition, the outlet gas of the reactor is bubbled in a Schlenk tube containing 0.8 mL of DMSO- $d_6$  (see Fig. S1). The solution is then transferred to a NMR tube and analyzed using a Bruker Avance III HD spectrometer operating at 500 MHz, equipped with a Prodigy cryoprobe. The full analysis consisted of  $^1\text{H}$ ,  $^{13}\text{C}$  Jmod,  $^{29}\text{Si}$  spin echo measurements, HSQC  $^1\text{H}$ - $^{13}\text{C}$ , HSQC  $^1\text{H}$ - $^{29}\text{Si}$ , HMBC and COSY pulse sequences. Using the same spectrometer, the commercially available by-products were analyzed in order to confirm their assignment.

The ESR analysis of the gas phase is performed using a KBr-POBN pellet. KBr is first desiccated in an oven at 80°C for 24 h. Then POBN (50 mg, 0.26 mmol) and KBr (330 mg, 2.8 mmol) are mixed and compacted together to form a pellet of 1 cm diameter. The pellet is placed inside the reactor at 78 cm from the inlet, where the local temperature measures 170°C. After deposition, the pellet is crushed and transferred into two ESR tubes. One is analyzed as is and the other is washed with toluene (2 mL), and the extracted liquid is analyzed. The two analyses are referred to as “solid phase” and “liquid phase” respectively hereinafter. The analysis of the solid and liquid phases is performed by conventional X-band ESR spectroscopy, using a Bruker Elexsys spectrometer equipped with a high-resolution cavity.

Accurate chemical composition data are provided by the use of Ion Beam Analysis (IBA) techniques, Rutherford Backscattering Spectroscopy (RBS), Nuclear Reaction Analysis (NRA) and Elastic Recoil Detection Analysis (ERDA), performed at the Pelletron facility of CEMHTI in Orléans, France. RBS and NRA are performed at a 166° detection angle with 2 MeV  $\alpha$  particles for the former. Oxygen, carbon and nitrogen concentrations are measured through the  $^{16}\text{O}(d,\alpha_0)^{14}\text{N}$ ,  $^{12}\text{C}(d,p_0)^{13}\text{C}$  and  $^{14}\text{N}(d,p_5)^{15}\text{N}$  nuclear reactions<sup>13</sup>, respectively, using incident deuterons of 0.9

MeV. ERDA measurements are performed using a 2.8 MeV alpha beam. For the measurement of hydrogen, the sample is positioned at a 15° grazing incidence angle and the recoiled hydrogen atoms are collected at a scattering angle of 30°. The overall composition of the films is obtained by simulating the RBS, NRA and ERDA acquire spectra using the SIMNRA software. The chemical structure of all identified compounds is generated by Avogadro version 1.20, an open-source molecular builder and visualization tool.<sup>34</sup>

### **3. Results and discussion**

#### **3.1. Thermal behavior of TDMSA precursor**

In order to analyze the thermal decomposition of TDMSA for the adopted operating conditions, constant flows of 2 sccm TDMSA and 4028 sccm N<sub>2</sub> were introduced in the CVD reactor at different temperatures in the range of 580-700°C and constant total pressure of 730 Torr. The adopted protocol is identical to the one of the CVD of films from TDMSA described in Section 2. The gas phase was collected with a sampling bag at the reactor exit for GC-MS analysis. **Figure 1** presents the conversion percent of the precursor after GC-MS quantification. The results are plotted as a function of the maximum temperature existing in the reactor chamber.

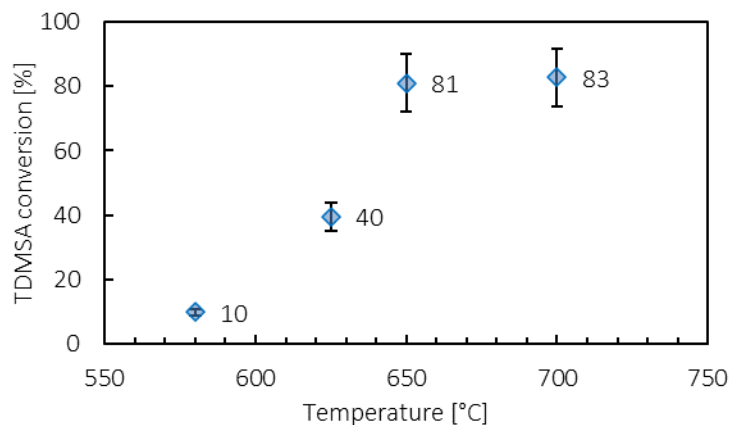


Figure 1. Evolution of the TDMSA conversion as a function of the temperature

At 580°C, only 10 % of the TDMSA introduced in the reactor is decomposed. Increasing the temperature from 580°C to 650°C increases the precursor decomposition from 10 to 81 %. Further increase of the temperature up to 700°C does not significantly influence the TDMSA conversion, which increases only slightly from 81 to 83 %. The curve reaches a plateau, indicating a possible recombination of the by-products, similarly to what was described by Knolle et al.<sup>35</sup> with the reformation of the tetramethyldisilazane (TMDSz) during its laser photolysis. Globally, the results indicate that TDMSA does not fully decompose in the probed temperature range, since it is always observed at the exit of the reactor. The study reveals that the decomposition of TDMSA is initiated at around 580°C and above, with the best compromise between a moderate deposition temperature and a high precursor conversion being 650°C. As such, the majority of the present study is carried out at this temperature (650°C), which is significantly lower than the usual 750-900°C range used for the CVD of SiO<sub>x</sub>N<sub>y</sub> films.<sup>13,36</sup> This confirms that the presence of Si-H bonds is favorable for activating the deposition mechanism at lower temperatures, thus decreasing the thermal budget of the process.

Qualitative GC-MS analysis indicated a number of by-products. Among many,  $(\text{Me}_2\text{HSi})_2\text{NH}$  (TMDSz) coexists with the starting silanamine precursor at 625°C. Then in the 650–700°C range, two supplementary by-products are identified, i.e. penta- and hexamethyldisilazanes  $(\text{Me}_2\text{SiH})\text{NH}(\text{SiMe}_3)$  (PMDSz) and  $(\text{Me}_3\text{Si})_2\text{NH}$  (HMDSz), respectively. The formation of these two compounds only at higher temperature is explained by their molecular structures containing a  $-\text{SiMe}_3$  moiety, which requires more energy and additional reaction steps to be formed from this particular starting precursor molecule. It is noted that the fluid dynamics of the current operating configuration can naturally influence the gas phase composition and distribution of identified species under the imposed conditions. However, the length of the reactor (i.e. 70 cm), the high dilution of the TDMSA precursor (i.e. 2 sccm TDMSA, 4028 sccm  $\text{N}_2$ -dilution), the elevated temperatures and the high residence time of the gas (>1.4 s) allow us to assume a complete mixing.

### 3.2. Thin films deposition

CVD experiments were carried out at 650°C, from TDMSA and  $\text{O}_2$ , with and without ammonia. For all experiments, the TDMSA flow rate and the process pressure were kept constant at 2 sccm and 730 Torr, respectively. In order to reach optimal conditions for the deposition of  $\text{SiO}_x\text{N}_y$ , the impact of the  $\text{NH}_3$  and  $\text{O}_2$  flow rates on the solid and gas phase composition is studied.  $\text{O}_2$  flow rate is varied from 0.3 to 1.2 sccm. Furthermore, for a fixed  $\text{O}_2$  flow rate of 0.6 sccm, three parameters are investigated: presence and absence of  $\text{NH}_3$  at 650°C, and deposition at 625°C in the absence of  $\text{NH}_3$ . **Table 1** presents the experimental conditions (temperature,  $\text{O}_2$  and  $\text{NH}_3$  flow rates) for each experiment, **Exp1** to **Exp6**, the resulting deposition rates measured by sample weighing and the nitrogen and carbon contents of the  $\text{SiO}_x\text{N}_y$  films determined by IBA, measured on a sample

located in the isothermal region of the reactor, positioned at ~38 cm from the inlet. The conversion percent of TDMSA, evaluated by quantitative GC-MS, is also included. The by-products identified in the gas phase by coupling GC-MS and NMR analyses are listed in **Table 2**, together with their respective enumeration and chemical structures where oxygen, nitrogen, carbon and silicon atoms are noted in red, blue, black and green, respectively. Independently of the inlet gas composition, the TDMSA precursor is present in the gaseous effluent, its conversion being at around 81 % for all experiments conducted at 650°C. Multiple by-products are observed and fifteen have been identified (Table 2). Identification of the chemical structure of these intermediary compounds gives interesting information to approach the deposition mechanism. Silanols (**1**, **4**, **5** and **9**) are observed, which can react directly with the silanol terminated surface sites of the substrate; disiloxanes (**3**, **6** and **9**), trisiloxanes (**11** and **12**), disilazanes (**7**, **10** and **13**) and even a mixed Si-N-Si-O-Si containing molecule (**15**) indicate the first steps of the silane condensation. Additional information of interest is the presence of by-products containing trimethylsilyl-substituted molecules (**2**, **4**, **6**, **8**, and **10**) in each of the previously cited families. Elimination of such compounds in the gaseous effluent is in agreement with the formation of the SiO<sub>x</sub>N<sub>y</sub> films, starting from the SiMe<sub>2</sub>H substitute molecule. The presence or absence of each of these by-products as a function of the experimental conditions will be discussed in the following sections, together with the respective film composition and deposition rate.

It is noted that the yield of the process was also taken into account, to discern the global balance between gas phase and surface reactions. By taking run Exp3 as an example (Table 1), 81 % of the supplied precursor is converted, in other words consumed, to produce gaseous by-products in the gas phase and thin film on the solid phase. Additionally, the silicon mass balance was calculated for the same experimental run (Exp3), considering deposition on all solid surfaces (reactor walls,

substrate holders, and substrates). Utilizing our available data (film composition, total deposited mass over a specific deposition duration and total TDMSA precursor supply for this duration), it was calculated that only a maximum of 1 % of the silicon supplied in the reactor is converted into solid thin film. Similar values were calculated for all other runs at 650°C (Exp1 to Exp5). When compared to the relatively high total conversion of the TDMSA precursor (80-86 %, Table 1), it becomes evident that gas phase reactions are more prominent than surface reactions. This is in coherence with the large number of silicon-containing by-products identified in the gas phase by GC-MS.

Table 1. Detailed deposition conditions and experimental results

	<b>Exp1</b>	<b>Exp2</b>	<b>Exp3</b>	<b>Exp4</b>	<b>Exp5</b>	<b>Exp6</b>
Temperature [°C]	650	650	650	650	650	625
O <sub>2</sub> flow rate [sccm]	0.6	0.6	0.6	0.3	1.2	0.6
NH <sub>3</sub> flow rate [sccm]	20	40	-	-	-	-
N at.% by IBA	6.3	6.2	5.8	9.8	4.7	4.5
C at.% by IBA	8.0	5.9	10.7	20.7	8.0	9.4
Deposition rate [mg min <sup>-1</sup> ]	1.4 10 <sup>-3</sup>	1.3 10 <sup>-3</sup>	1.6 10 <sup>-3</sup>	1.0 10 <sup>-3</sup>	2.1 10 <sup>-3</sup>	1.4 10 <sup>-3</sup>
TDMSA conversion [%]	81	80	81	86	82	59

### 3.2.1. Deposition in presence of NH<sub>3</sub> and O<sub>2</sub>

Exp1 was carried out at 650°C and 0.6 sccm of O<sub>2</sub>, in presence of NH<sub>3</sub> serving as nitrogen source. The films are deposited with a 1.4 10<sup>-3</sup> mg min<sup>-1</sup> rate and contain 6.3 at.% N and 8.0 at.% C. It will be shown, by FT-IR analysis, in a forthcoming publication that carbon is incorporated as CH<sub>3</sub> in the obtained SiO<sub>x</sub>N<sub>y</sub> films. For these operating conditions, the gas phase contains TDMSA precursor and at least 10 by-products identified (Table 2). These by-products are silanols (**1** and **4**), siloxanes (**3**, **6**, **9**, **11**, **12**), disilazane (**7**), silanamine (**15**) and water. Multiple compounds observed



by GC-MS are also encountered in NMR. Interestingly, NMR study allows to evidence the formation of water in this experiment contrary to the GC-MS analysis, for which the identification of H<sub>2</sub>O is prevented by its low molecular mass and short retention time.

Table 2. Enumeration and chemical structure of compounds identified by GC-MS and NMR depending on the operating conditions.

N°	Chemical structure	Abbreviation	Exp1	Exp2	Exp3	Exp4	Exp5	Exp6
0		-	✓	✓	✓	✓	✓	✓
1		-	✓	✓	✓			
2		MeOTMS			✓	✓	✓	
3		TMDSO	✓	✓	✓	✓	✓	
4		-	✓	✓	✓	✓	✓	✓
5		-			✓			
6		PMDSO	✓		✓			
7		TMDSz	✓		✓	✓	✓	✓
8		PMDSz			✓	✓		
9		-	✓	✓	✓			✓
10		HMDSz				✓		
11		HMTSO	✓	✓	✓	✓	✓	✓
12		HMCTSO	✓		✓	✓	✓	✓
13		-			✓		✓	✓
14		TDMSA	✓	✓	✓	✓	✓	✓
15		-	✓	✓	✓		✓	✓

**Figure 2** presents the  $^1\text{H}$  NMR spectrum of the gaseous effluent of Exp1. Due to the variety and multitude of products, analysis is made complex and difficult, requiring various NMR sequences for the accurate assignment of the main products. Despite this complexity, the  $^1\text{H}$  NMR spectra (Figure 2a) systematically show two main zones: one encountered from -0.01 to 0.22 ppm (Figure 2b) and the other in the 4.60 - 4.72 ppm range (Figure 2c). The former is assigned to the methyl resonance of Si-CH<sub>3</sub> moieties, while the latter corresponds to that of hydrogen atoms of Si-H fragments. In the Si-CH<sub>3</sub> zone, singlets are assigned to trimethyl substitutes and doublets, due to the presence of the  $J_{\text{HH}}^3$  coupling constant, indicate HSi(CH<sub>3</sub>)<sub>2</sub> groups. Even if complete assignment is not possible, compounds **3**, **4**, **6**, **7** and **11** are accurate by comparing with commercial sources. A few additional compounds seem to be hidden underneath other peaks. The low conversion percent and the presence of -SiMe<sub>2</sub> or -SiMe<sub>3</sub> moieties in the molecules in the gas phase are coherent with the formation of a silicon oxynitride SiO<sub>x</sub>N<sub>y</sub> film containing carbon in aliphatic form. This observation is also in agreement with the results reported by Lee et al.<sup>37</sup> and Gonzalez-Luna et al.,<sup>38</sup> indicating that trimethylsilyl derivatives such as HMDSz enhance the carbon content of silicon oxynitride films. In the present work, only two molecules containing -SiMe<sub>3</sub> moiety (**4**, **6**) have been identified in the gas phase in presence of ammonia, indicating that NH<sub>3</sub> could prevent the incorporation of methyl groups in the films.

Increasing, the NH<sub>3</sub> flow rate from 20 sccm (Exp1) to 40 sccm (Exp2) does not modify the nitrogen content of the SiO<sub>x</sub>N<sub>y</sub> films, which remains at 6.2 at.% N. This indicates that the nitrogen in the films is not linked to the concentration of NH<sub>3</sub> in the input gas or that the latter is already saturated at 20 sccm NH<sub>3</sub>.

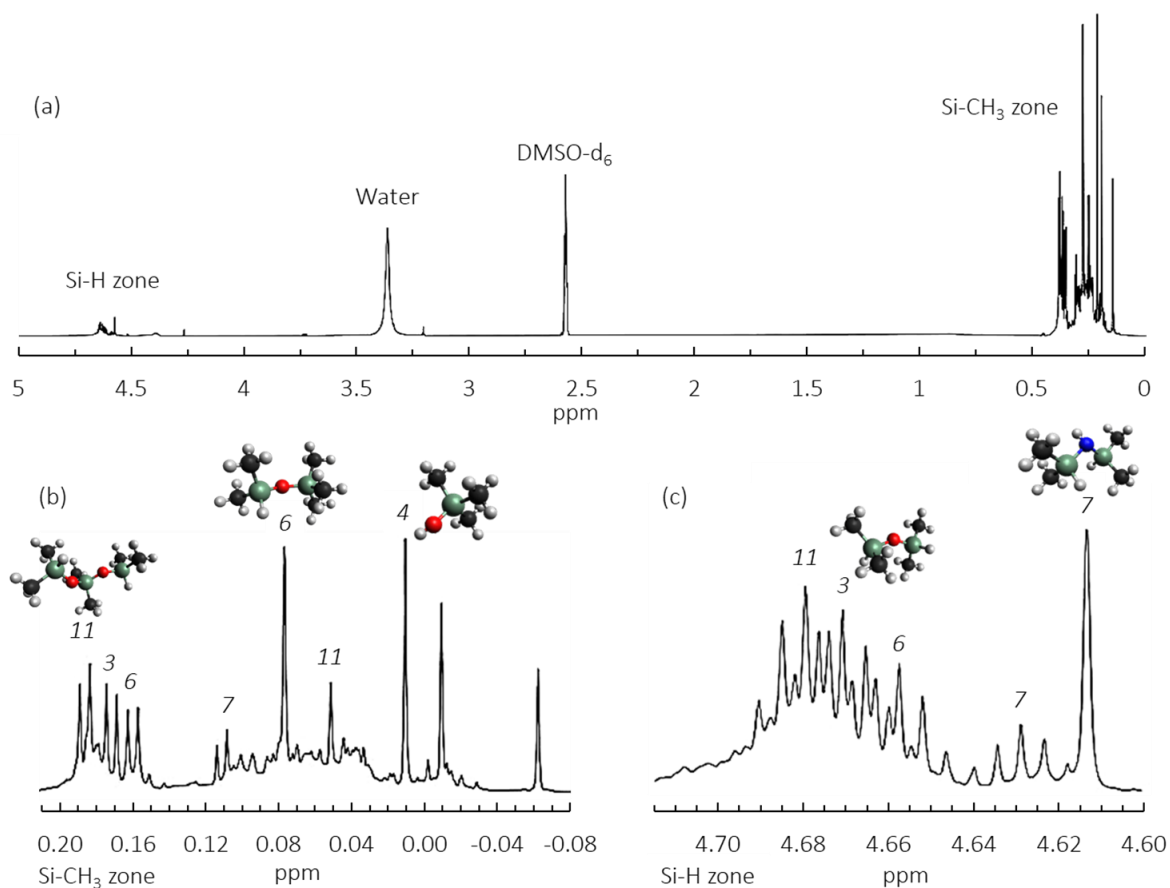


Figure 2. NMR spectrum of Exp1 (a) ; zoom in the 4.60-4.72 ppm (b) and -0.01-0.22 ppm (c) range, 500 MHz in DMSO- $d_6$ .

Removing ammonia from the gas phase (Exp3) yields surprising results. The nitrogen content slightly decreases, however the films still contain 5.8 at.% N (Table 1). This indicates that the nitrogen in the films originates from TDMSA. It is concluded that dimethylsilylamine derivatives containing H-Si-N bonds, such as TDMSA, can be helpful in obtaining silicon oxynitride films at temperatures lower than 700°C, without the requirement to add ammonia in the starting chemistry. This particular ability of such precursor molecules can be related to their molecular structure and is in agreement with results reported by Wrobel et al.,<sup>14</sup> who highlighted that precursors lacking Si-H bonds in their structure are less reactive and require higher energies to overcome their activation step for Si<sub>3</sub>N<sub>4</sub> or SiO<sub>x</sub>N<sub>y</sub> film formation. This renders molecules such

as HMDSz less reactive than TDMSA, since the latter contains three Si-H bonds and the former none. In a similar context, Tomar et al.<sup>39</sup> reported that the Si<sub>3</sub>N<sub>4</sub> deposition from HMDSz at 780°C requires ammonia as a nitrogen source, in contrast to the present work, where SiO<sub>x</sub>N<sub>y</sub> films were formed from TDMSA in absence of NH<sub>3</sub> and at lower temperatures. In addition, both the precursor conversion percent and the average deposition rate remain unchanged, regardless of the presence or not of NH<sub>3</sub> in the inlet gas for similar O<sub>2</sub> flow rate and deposition temperature. In contrast, the carbon content of the films significantly increases under an ammonia-free atmosphere, suggesting that the key role of ammonia in the studied chemistry is to participate in the reduction of carbon incorporation in the film rather than to provide nitrogen, in agreement with previous works from Xia et al.<sup>40</sup> and Tijanic et al.<sup>41</sup> among others. The increase of the carbon content (from 8.0 to 10.7 at.%) and the slight decrease of nitrogen content (from 6.3 to 5.8 at. %) in absence of NH<sub>3</sub> (Exp3) could therefore be linked to the larger number of compounds formed in Exp3, compared to Exp1 where NH<sub>3</sub> is present. As shown in Table 2, in addition to the compounds previously observed in Exp1 (presence of NH<sub>3</sub>), new by-products methoxytrimethylsilane MeOTMS (**2**), dimethylsilanediol (**5**) and the silanamines PMDSz (**8**) and (**13**) are observed for Exp3. Among these, compounds **2**, **4**, **6** and **8** are trimethylsilane derivatives, which could be held accountable for the higher carbon content in the film. This is in coherence with Xia et al.,<sup>40</sup> who reported that reduction of carbon incorporation in silicon nitride or silicon oxynitride films depends on the use of dimethylsilane derivative precursors instead of trimethylsilyl ones.

With 40 sccm of ammonia (Exp2), a further decrease in carbon content is observed (5.9 at. % C) whereas the nitrogen content is similar to Exp1. The relatively low and stable nitrogen incorporation under the various NH<sub>3</sub> flow rates confirms that NH<sub>3</sub> does not participate in enriching the films with nitrogen. Fewer by-products are observed for Exp2, with only compounds **1**, **3**, **4**, **9**,

**11**, **14** and **15** being identified. Among these molecules, only **4** is a SiMe<sub>3</sub> containing derivative, which correlates well with the overall lower carbon content in the films in comparison to Exp1 and Exp3. It is therefore evident that higher NH<sub>3</sub> flow rates reduce the number of by products and more importantly results in less trimethylsilyl compounds in the gas phase and consequently, leads to films with lower carbon content. However, no enrichment in nitrogen is observed. As such, the non-requirement of NH<sub>3</sub> as a nitrogen source is highlighted, in chemistries where a silicon and nitrogen-containing molecule such as TDMSA is used as the precursor. This allows the chemical system to be simplified and utilize the combination of only O<sub>2</sub> as oxidant and TDMSA, with the latter fulfilling the dual role of silicon and nitrogen provider. Moreover, SiO<sub>x</sub>N<sub>y</sub> deposition is enabled at 650°C thanks to the presence of Si-H bonds in the starting molecule.

### 3.2.2. Influence of the O<sub>2</sub> flow rate in absence of NH<sub>3</sub>

The impact of the O<sub>2</sub> flow rate on the chemical composition of the deposited films as well as of the gas phase was studied for O<sub>2</sub> flow rates of 0.3 (Exp4) and 1.2 sccm (Exp5) and is compared to the reference experiment Exp3 with 0.6 sccm O<sub>2</sub> (Table 1 and 2). As expected, when the O<sub>2</sub> flow rate is decreased from 0.6 to 0.3 sccm, the deposition rate of SiO<sub>x</sub>N<sub>y</sub> decreases from 1.6 10<sup>-3</sup> to 1.0 10<sup>-3</sup> mg min<sup>-1</sup>. This decrease can be explained by the decrease of oxygen atoms available in the reactive gas phase. At the same time, the nitrogen content of the films increases from 5.8 at.% (Exp3) to 9.8 at.% (Exp 4), indicating the more pronounced nitride character of the material. These results on the solid phase are a reflection of the changes induced in the gas phase. The decrease of the O<sub>2</sub> concentration in the input gas impacts the global gas phase composition, with a decrease in the number of by-products observed by NMR and GC-MS (Table 2). For the lower O<sub>2</sub> flow (Exp4), dimethylsilanediol **5**, disiloxanes **6** and **9** and silanamines **13** and **15** are not detected, their absence being attributed to the lower oxygen flow rate. Naturally, a lower oxygen concentration in the gas

phase translates to less oxidation of Si-C or Si-N bonds, which in turn are then free to participate in the formation of disilazanes TMDsZ (**7**) and HMDSz (**10**) and the silanamine PMDSz (**8**). Consequently, the presence of these compounds in the gas phase explains the higher nitrogen and carbon content of the films, given that they contain N-SiMe<sub>2</sub> and/or N-SiMe<sub>3</sub> moieties.

On the contrary, when the oxygen flow rate is increased from 0.6 to 1.2 sccm across Exp3 and Exp5, respectively, the opposite trend can be observed regarding the deposition rate and the N and C contents of the films (Table 1). Firstly, the higher O<sub>2</sub> flow in Exp5 results in a higher deposition rate, as expected. In terms of gaseous by-products, increase O<sub>2</sub> supply facilitates the oxidation of Si-N or Si-C bonds and results in fewer nitrogen containing compounds compared to Exp3 and Exp4. The compounds identified for Exp5 are silanol **4**, methoxytrimethylsilane **2**, disiloxane **3**, disilazane **7**, trisiloxanes **11** and **12**, silanamines **13** and **15** (Table 2). Compounds **13** and **15**, composed of a -Si-N-Si-O-Si bonding sequence, seem to be convenient intermediary compounds for the formation of the SiO<sub>x</sub>N<sub>y</sub> film.

In summary, variation of the O<sub>2</sub> flow rate affects the nitrogen percentage in the film as follows: increase of the O<sub>2</sub> flow rate leads to the production of multiple siloxane products in the gas phase, which in turn readily participate in the formation of SiO<sub>2</sub> material. The oxide character of the films is increased and the nitrogen content decreases in relation to it. This is also a consequence of the lower amount of nitrogen-containing silanamine by-products in the gas phase. In the same way, by reducing the oxygen flow rate, the formed film has a higher nitrogen content, which is also reflected in the presence of additional nitrogen containing gaseous by-products.

An interesting point of observation is that for all experiments performed at 650°C, the TDMSA conversion remains around 81%. This could hint that oxygen is not participating in the

activation of TDMSA, and that the temperature seems to be the main parameter influencing the TDMSA conversion.

### *3.2.3 Depositions at 625°C*

An experiment at 625°C has been undertaken (Exp6), exploring the possibility to decrease the temperature of the CVD process and to investigate the resulting gas phase. Based on the thermal behavior of TDMSA (Figure 1), a conversion of approximately 40 % is expected in absence of O<sub>2</sub> at this temperature. Interestingly, the addition of 0.6 sccm of O<sub>2</sub> in Exp6 results in a conversion of around 59 %. Both conversion percentages are lower than the one noted at 650°C. However, it is important to underline that at 625°C, an oxygenated atmosphere leads to a higher conversion of TDMSA. As a conclusion, for the adopted process conditions, the temperature is the only parameter that has an impact on the precursor conversion at 650°C, whereas at just 25 degrees lower temperature, addition of oxygen increases the TDMSA conversion. The participation of oxygen in the precursor conversion at lower temperature hints at a potentially different reaction pathway compared to the one followed at 650°C.

Regarding the average deposition rate and the N and C content of the films, all values were noted to decrease when the temperature was lowered from 650°C (Exp3) to 625°C (Exp6). This is a direct consequence of the lower precursor conversion percent at 625°C, which also influences the gas phase composition. Fewer by-products (**4**, **7**, **9**, **11-15**) are observed at 625°C, as a result of two potential reasons. The lower conversion of the precursor results in a lower concentration of species that can act as the building blocks for the formation of additional by-products, and/or it is not possible to form the latter due to the decrease in supplied energy (i.e., lower deposition temperature).



### 3.3. Mechanistic investigation

#### 3.3.1. ESR study of radical intermediates

ESR study was performed in order to gain further insight into the deposition mechanism. In order to observe reactive species such as radicals, a spin-trap molecule was encapsulated in a KBr pellet. The advantages of this methodology are first to allow the thermal protection of the organic spin-trap molecule, and second to avoid dispersion of the spin-trap powder within the reactor. A spin-trap with a decomposition temperature high enough to allow its use inside the reactor was found to be  $\alpha$ -(4-pyridyl-1-oxide)-N-tert-butyl nitron (POBN). For each experiment, independently of the reaction conditions (presence or absence of ammonia, O<sub>2</sub> flow rate or temperature), the same radical species was systematically trapped. **Figure 3** shows typical ESR spectra obtained in liquid and solid states with g-factor equal to 2.0059. In the solid state spectrum, the signal observed is anisotropic with  $g_x=2.021$ ,  $g_y=2.005$  and  $g_z=1.984$ . After extraction in toluene, a liquid state spectrum was recorded, showing more clearly a triplet signal with an average g of 2.0059. The liquid state also gives access to the hyperfine constants  $a_N=14.6$  G whereas  $a_H$  is confounded in the bandwidth.

The similarity between the ESR spectra of Exp1 to Exp6 for both liquid and solid phases across the various operating conditions indicates a common radical generation. This emphasizes its origin from the precursor, as well as its independence from the other reactants used in the inlet gas composition. Additionally, it is noted that since the decomposition of the precursor is predominantly thermally activated, it can give rise to multiple pathways based on homolytic dissociation of the different bonds describing the precursor molecule. For example, the homolytic breaking of the Si-N bond, Equation (1), would result in the formation of  $Me_2HSi^\circ$  and

(Me<sub>2</sub>HSi)<sub>2</sub>N° radicals, noted hereinafter *Si\_int*° and *N\_int*°, respectively, while that of the Si-H bond, Equation (2) would form H° and a hindered Si-centered radical. Finally, if the pathway began with the Si-C bond, it would produce a CH<sub>3</sub>° and another hindered Si-centered radical, Equation (3).

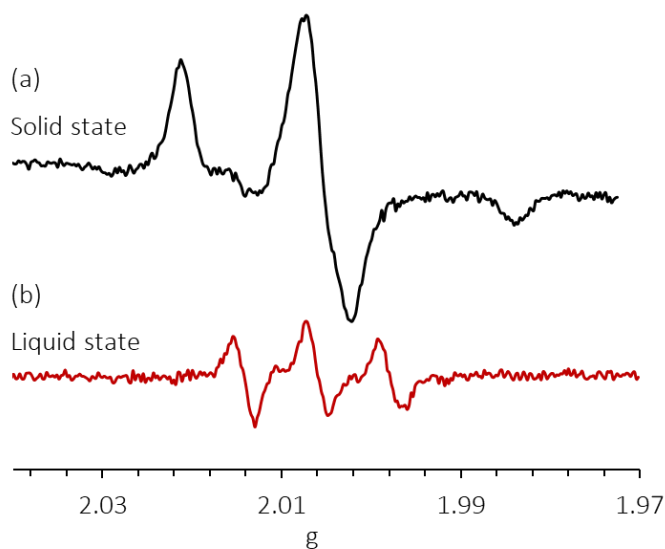
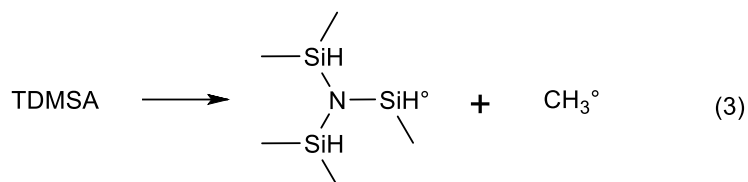
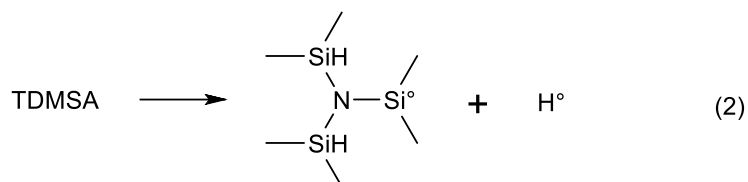
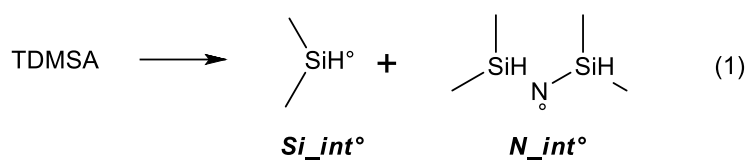


Figure 3. ESR spectra of POBN-R° (Exp3) at the solid (a) and liquid (b) state



Because of their very short lifetime, methyl and hydrogen radicals are not the paramagnetic species trapped by POBN. Moreover, the hyperfine structure of the signal together with the  $g$  value observed ( $g=2.0059$ ,  $a_N=14.6$  G), is not consistent with the referenced data reported for  $\text{CH}_3^\circ$  ( $g=2.0035$ ,  $a_N=14.98$  G,  $a_H=2.46$  G)<sup>42</sup>  $\text{H}^\circ$  ( $a_N=16.2$  G,  $a_H=10.2$  G).<sup>43</sup> In the case of the  $(\text{Me}_2\text{HSi})_2\text{N}^\circ$  radical, a more complex hyperfine structure (comprised of 18 lines) would be expected.<sup>35</sup> Thus, the measured  $g$  value is assumed to be related to a silicon-centered radical, in agreement with data reported for radicals such as  $\text{SiHMe}_2^\circ$  or  $\text{SiMe}_3^\circ$  trapped by  $\alpha$ -phenyl-*N*-*tert*-butyl nitron (PBN)<sup>44</sup>,<sup>45</sup> characterized by a  $g$ -factor of  $2.0059\pm 0.0001$ . Nevertheless, the Si-centered radicals resulting from the cleavage of the Si-C or Si-H bond, Equation (2) and (3) respectively, are unlikely to be trapped, as they are hindered molecules. Thus, the above hypothesis is in favor of the formation of the  $\text{Me}_2\text{HSi}^\circ$  radical through Equation (1), in agreement with the presence of **1**, **2**, **4** and **5** monosilylated derivatives involving in their formation a  $\text{Me}_2\text{HSi}$ - moiety as a building block. The reaction of the two hindered Si-centered radical molecules (produced from Equations 2 and 3) with POBN is not excluded. However, the resulting adducts are considered unstable, in a sense that they can easily rearrange (hydrogen shifts) and decompose through a dissociation of the Si-N bond, leaving behind only a monosilylated fraction of the original radical. For that reason, it is proposed that there is a high probability that all adducts eventually lead to the trapping of the  $\text{Me}_2\text{SiH}^\circ$  radical.

### 3.3.2. Proposition of a deposition mechanism

In this sub-section, an apparent deposition mechanism is proposed based on the consideration of all previously mentioned gas phase and films characterization results. The homolytic cleavage of the TDMSA precursor is considered as the first reaction step toward the eventual deposition of a  $\text{SiO}_x\text{N}_y$  film. Three distinct homolytic cleavage reactions were proposed

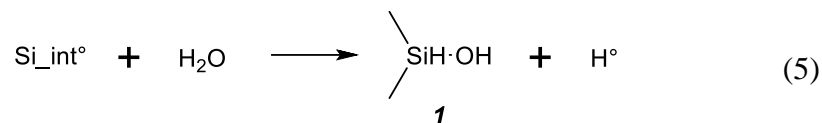
in section 3.3.1, with the  $\text{Me}_2\text{HSi}^\circ$  radical produced through Equation (1) being the one trapped using POBN. However, the presence of trimethylsilane-containing compounds **4**, **6** and **10**, among others, indicates an additional Si-CH<sub>3</sub> bond cleavage through Equation (3), while compounds **7** and **15** possess one extra hydrogen atom, potentially resulting from the Si-H bond cleavage, Equation (2). So, even if these radical species ( $\text{H}^\circ$ ,  $\text{CH}_3^\circ$ ) were not evidently trapped with POBN, their presence can still be assumed given their high reactivity. As a result, Equation (1) is proposed to be the primary pathway and first reaction step of the mechanism, with Equation (2) and Equation (3) taking place in parallel, albeit at slower rates.

#### *In the gas phase*

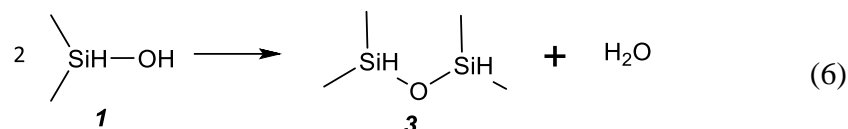
Multiple reactions in the gas phase can take place involving  $\text{Si\_int}^\bullet$ ,  $\text{N\_int}^\bullet$ ,  $\text{H}^\circ$  and  $\text{CH}_3^\circ$  radicals resulting from the decomposition of TDMSA. Being in an oxidizing atmosphere, it is proposed that  $\text{Si\_int}^\circ$  produced through Equation (1) reacts with the diradical  $\text{O}_2$  to form a peroxy radical  $\text{Me}_2(\text{H})\text{SiOO}^\circ$ , followed by the formation of a  $\text{Me}_2(\text{H})\text{SiOOH}$  peroxide. After homolysis of the relatively weak O-O bond of the peroxide, the resulting silyloxy radical  $\text{Me}_2(\text{H})\text{SiO}^\circ$  can lead to the production of silanol compound **1** by  $\text{H}^\circ$  abstraction as shown in Equation (4).

To insert peroxide equation here (4)

Although no peroxide compounds were detected by GC-MS, their presence is not excluded, given that the He injection port is at 250°C. In an alternative route,  $\text{H}^\circ$  could form water with  $\text{O}_2$ , which will in turn react with  $\text{Si\_int}^\bullet$  to form compound **1**, Equation (5), although it is considered that this reaction is taking place at slower rates.

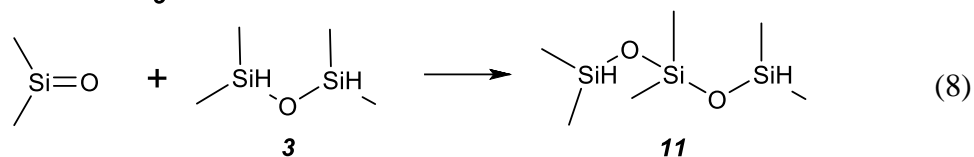
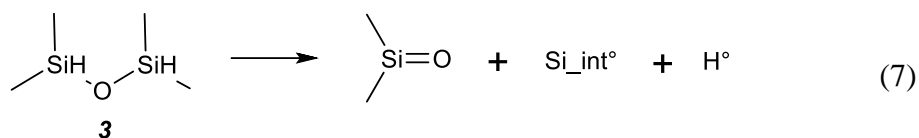


Reaction of the silanol compound **1** with an oxygen radical can lead to the production of the silanediol compound **5**, as shown in Equation (4). Moreover, the condensation of two silanol molecules, **1**, produced according to Equations (4) or (5), can then result in the formation of compound **3**, Equation (6).

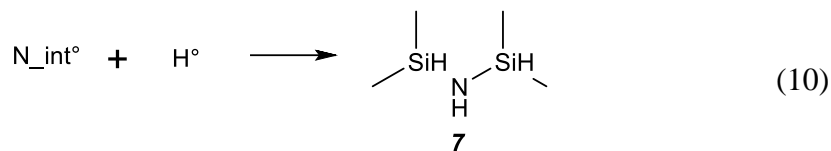
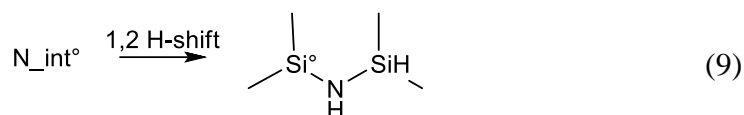


As suggested by Pola et al.,<sup>46</sup> siloxane molecules can disproportionate into a silanone and a radical species when given enough energy, with the radical species participating in the polymerization of other siloxane molecules. Following this proposition, compound **3** is assumed to yield *Si\_int*<sup>•</sup>, H<sup>•</sup> and a dimethylsilanone through Equation (7). The radical species H<sup>•</sup> and *Si\_int*<sup>•</sup> can additionally react together to form dimethylsilane. This compound is not observed in the gas phase; however, it is highly reactive and can be potentially formed. Moreover, being in an oxidizing atmosphere, dimethylsilane could be oxidized into silanol compounds such as **1** and **5**. The newly formed silanols can in turn participate in the formation of **3** through Equation (6), producing a continuous cycle between Equations (4) and/or (5) with (6) and (7).

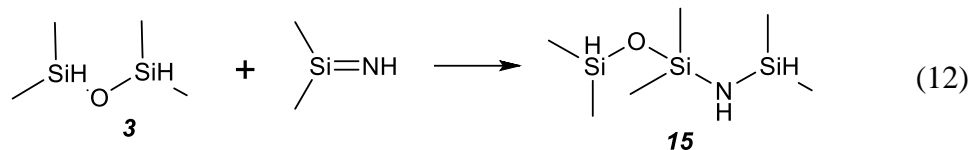
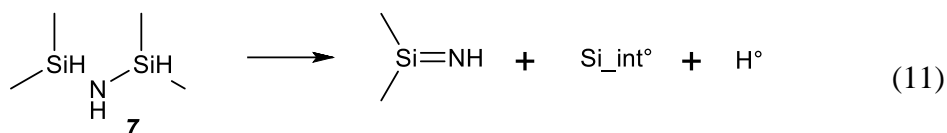
The silanone formed through Equation (7) is then used to polymerize TMDSO **3** into HMDSO **II** through Equation (8).



It is recalled that decomposition of TDMSA through Equation (1) also yields  $N\_int^\bullet$ . This radical compound can undergo a 1,2 H-shift, yielding a new Si-centered radical,<sup>35</sup> Equation (9), or it can react with a  $H^\bullet$  leading to the formation of TMDSz **7**, Equation (10). All of the detected nitrogen-containing by-products (**Table 2**) feature a hydrogenated nitrogen atom, further supporting the 1,2 H-shift. Moreover, the formation of the new Si-centered radical through this 1,2 H-shift could in fact explain why only Si-centered species are identified by ESR, despite Equation (1) yielding two different radical species ( $Si\_int^\bullet$  and  $N\_int^\bullet$ ).

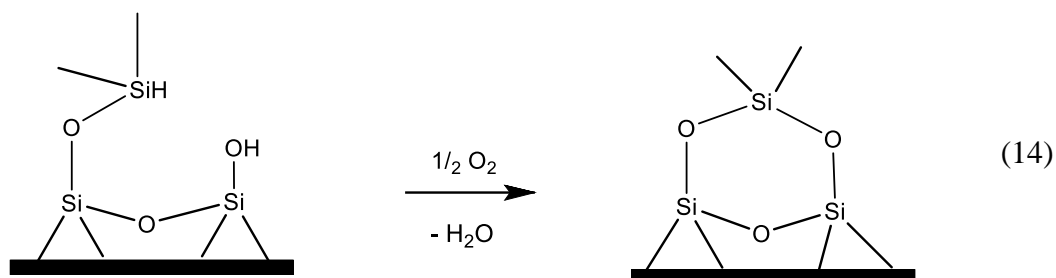
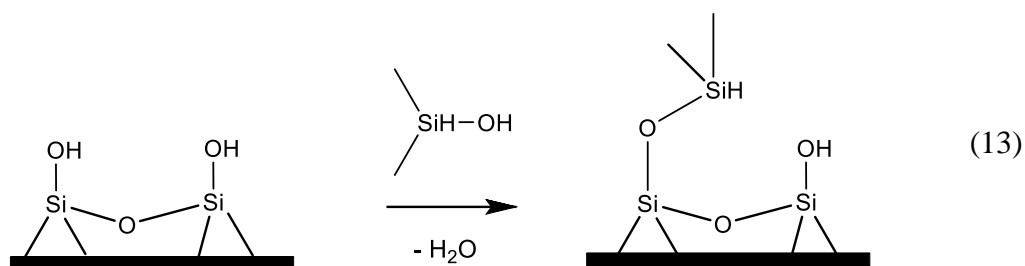


Following the same reasoning as for TMDSo **3**, TMDSz **7** can also disproportionate and yield  $Si\_int^\bullet$ ,  $H^\bullet$  and a silanimine, Equation (11), which can in turn be used to polymerize siloxanes and drive the formation of bi-functional compounds with a –Si-N-Si-O-Si sequence such as **15**, Equation (12). The presence of **15** in the gas phase even in absence of  $NH_3$ , emphasizes the participation of TDMSA in the formation of silicon oxynitride films.



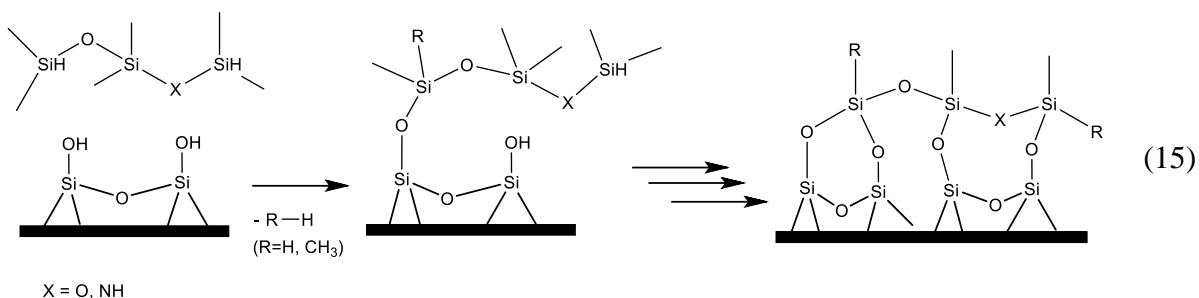
### Film formation

$\text{Si\_int}^\bullet$  is present in the gas phase in large concentrations, produced from Equation (1), (7) and (11), it can be involved to form silica film by reacting with the silanol sites of the substrate surface, as illustrated in Equation (13) and (14). The siloxane formed in Equation (13), can then be oxidized by oxygen from the gas phase before reacting with the geminal silanol on the substrate, Equation (14).



The low amount of nitrogen in the film suggests a major incorporation of oxygen with siloxane compounds **3**, **6** and **12**, Equation (13) and (14), while the incorporation of nitrogen is

only possible through a few molecules such as **13** and **15**. In Equation (15), a general mechanism for the formation of  $\text{SiO}_x\text{N}_y$  film from trisiloxane **11** ( $\text{X}=\text{O}$ ) and silanamine **15** ( $\text{X}=\text{NH}$ ) is proposed. The adsorption mechanism of these molecules from the gas phase onto the substrate is similar to Equation (13) and (14), but will result in the formation of a silicon oxynitride film in the case of molecules such as **15**, containing a Si-N-Si-O-Si- sequence, Equation (15). The first step when **15** is reacting with the substrate is the formation of an O-Si bond (stronger than a N-Si one), which can act as the driving force of the deposition mechanism.



The proposed simplified mechanism paves the way to the kinetic numerical modelling of the studied TDMSA-O<sub>2</sub> CVD process. The aim of modelling such system is (i) the optimization of the deposition conditions and of the reactor geometry to uniformly treat various substrates, whether they are planar or more complex and to reach target film thickness and composition, (ii) to help the process scale up.

#### 4. Conclusion

Simultaneous analysis of the gas phase during the APCVD of silicon oxynitride from tris(dimethylsilyl)amine (TDMSA) involving chemistries was carried out, using a combined GC-MS, ESR and NMR investigation. This novel methodology, implemented for the first time in such



CVD process allows understanding the impact of the molecular structure of the starting silane precursor on the CVD operating conditions and the stoichiometry of the formed film. The combined detailed analysis by CG-MS and NMR highlighted the wealth of the gas phase chemistry and its evolution as a function of the investigated process conditions.

Through quantitative GC-MS analysis, it was found that the TDMSA precursor decomposes in the 580-700°C range in absence of oxygen. For temperatures higher than 650°C, decomposition of the precursor is purely temperature-driven, but for lower temperatures, a higher conversion is observed upon the addition of O<sub>2</sub>.

The overall molecular structure of the precursor and the multiple potential decomposition pathways underlie the complexity of the gas phase, giving rise to a large number of gaseous by-products. Variation of the operating conditions lead to the detection of up to 15 compounds in the gas phase and the production of films with varying compositions. An increase of the O<sub>2</sub> flow rate leads to the production of multiple siloxane products in the gas phase, which was reflected in a more pronounced oxide character of the films. In contrast, by reducing the O<sub>2</sub> flow rate, additional nitrogen containing gaseous by-products were detected in the gas-phase, the deposited film has a higher nitrogen content, which is also reflected in the presence of. Interestingly, fewer numbers of by-products were detected when NH<sub>3</sub> was added in the inlet chemistry, which was proposed to be the reason for the lower carbon impurities found in the SiO<sub>x</sub>N<sub>y</sub> films under NH<sub>3</sub> flow.

A significant result was the deposition of silicon oxynitride films even in absence of ammonia, demonstrating the judicious choice of the TDMSA silanamine as a dual source of nitrogen and silicon. No synergetic effect of ammonia addition in the TDMSA-O<sub>2</sub> system was observed in terms of nitrogen content modulation for the tested operating conditions. Additionally,

the presence of Si-H bonds in the precursor structure renders it possible to form SiO<sub>x</sub>N<sub>y</sub> films by thermal CVD, at temperatures lower than those required by other conventional silazane/silanamine precursors such as HMDSz. As a result, it is demonstrated that the TDMSA precursor, or molecules with a similar structure (presence of N-Si-H bonds), can open the way to new developments of silicon oxynitride deposition processes without requiring NH<sub>3</sub>, thus simplifying system complexity.

Finally, the combined study of the gas phase using GC-MS, NMR and ESR provided insight in the deposition mechanism. The decomposition of the TDMSA precursor through a homolytic cleavage of its Si-N bond was narrowed down through the detection of a silylated Me<sub>2</sub>HSi° radical by ESR. Consideration of the decomposition pathways and the by-products identified in the gas phase allowed the proposal of multiple potential reactions highlighting the mechanisms involved in the solid film formation. These results open the way to develop a kinetic numerical model of the CVD process aiming to find optimized deposition conditions or reactor geometry to coat planar or more complex substrates for targeted applications. The methodology developed in this work to characterize the gas phase at the reactor exit can now be applied to other chemical systems in the vision of CVD process development and optimisation.

### *Acknowledgements*

The present work was funded by the French Agence Nationale de la Recherche (ANR) under the Contract HEALTHYGLASS ANR-17-CE08-0056. The authors are indebted to Lionel Rechart, LCC UPR and Eric Leroy, ICT for fruitful discussions on ESR and GC-MS analyses respectively. Anonymous reviewers are also acknowledged for their constructive comments and suggestions.

*Conflict of Interest*

The authors declare no conflicts of interest.

## Supporting Information

### **An innovative GC-MS, NMR and ESR combined, gas-phase investigation during chemical vapor deposition of silicon oxynitrides films from tris(dimethylsilyl)amine**

*Laura Decosterd, Konstantina C. Topka, Babacar Diallo, Diane Samelor, Hugues Vergnes, François Senocq, Brigitte Caussat, Constantin Vahlas, Marie-Joëlle Menu\**

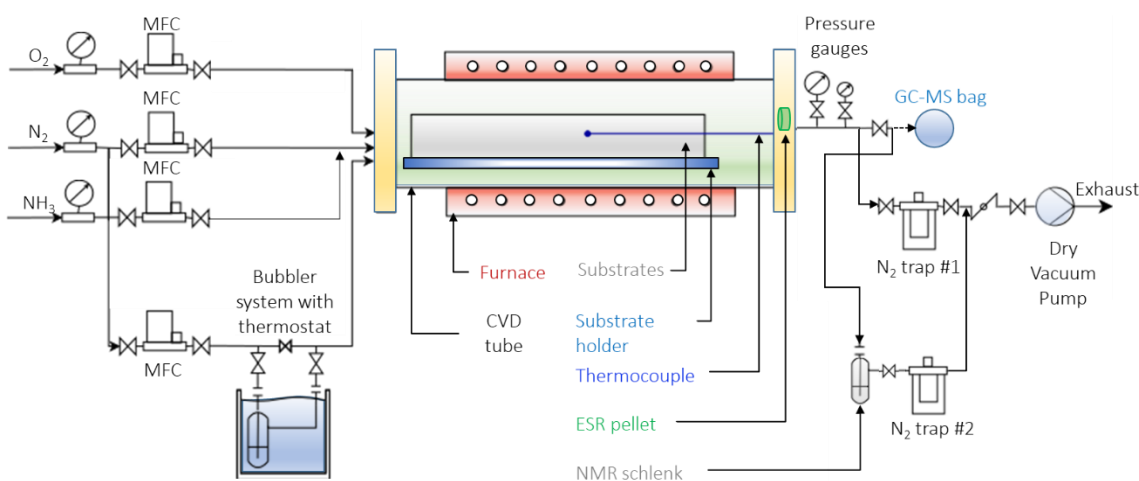


Figure S1. Schematic representation of the tubular CVD reactor

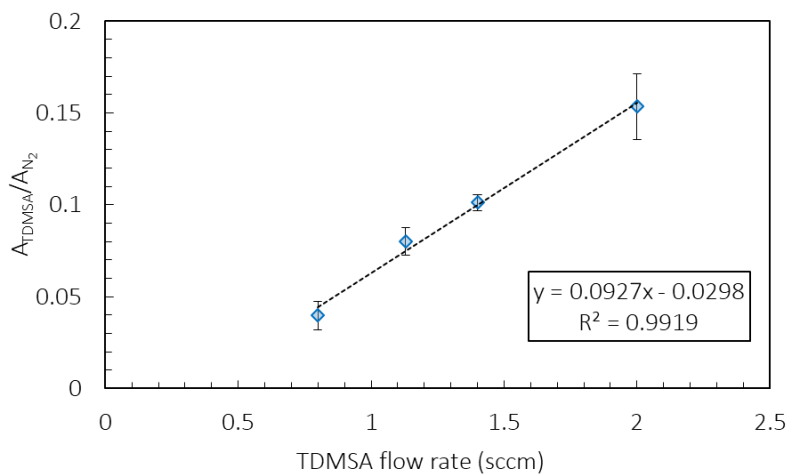


Figure S2. Calibration curve of TDMSA

## Abbreviations

TDMSA	Tris(dimethylsilyl)amine
HMDSz	Hexamethyldisilazane
BTBAS	Di( <sup>t</sup> butylamino)silane
APMDES	3-aminopropylmethyldiethoxysilane
TEOS	Tetraethoxysilane
TSA	Trisilylamine
TMDSz	1,1,3,3-tetramethyldisilazane
TDMAS	Tris(dimethylamino)silane
PMDSz	Pentamethyldisilazanes,
MeOTMS	Methoxytrimethylsilane
TMDS <sub>o</sub>	1,1,3,3-Tetramethyldisiloxane
PMDS <sub>o</sub>	Pentamethyldisiloxane
HMTS <sub>o</sub>	Hexamethyltrisiloxane
HMCTS <sub>o</sub>	Hexamethylcyclotrisiloxane
POBN	$\alpha$ -(4-pyridyl-1-oxide)-N-tert-butyl nitron

## References

1. Y. Shi, L. He, F. Guang, L. Li, Z. Xin and R. Liu, A review: preparation, performance, and applications of silicon oxynitride film, *Micromachines*, 2019, **10**, 552.
2. M. Shahpanah, S. Mehrabian, M. Abbasi-Firouzjah and B. Shokri, Improving the oxygen barrier properties of PET polymer by radio frequency plasma-polymerized SiO<sub>x</sub>N<sub>y</sub> thin film, *Surface and Coatings Technology*, 2019, **358**, 91-97.
3. Z. Zhang, Z. Shao, Y. Luo, P. An, M. Zhang and C. Xu, Hydrophobic, transparent and hard silicon oxynitride coating from perhydropolysilazane, *Polymer International*, 2015, **64**, 971-978.
4. Y. Shima, H. Hasuyama, T. Kondoh, Y. Imaoka, T. Watari, K. Baba, et al., Mechanical properties of silicon oxynitride thin films prepared by low energy ion beam assisted deposition, *Nuclear Instruments and Methods in Physics Research Section B: Beam Interactions with Materials and Atoms*, 1999, **148**, 599-603.
5. E. K. Park, S. Kim, J. Heo and H. J. Kim, Electrical evaluation of crack generation in SiN<sub>x</sub> and SiO<sub>x</sub>N<sub>y</sub> thin-film encapsulation layers for OLED displays, *Applied Surface Science*, 2016, **370**, 126-130.
6. P. Temple-Boyer, B. Hajji, J. Alay, J. Morante and A. Martinez, Properties of SiO<sub>x</sub>N<sub>y</sub> films deposited by LPCVD from SiH<sub>4</sub>/N<sub>2</sub>O/NH<sub>3</sub> gaseous mixture, *Sensors and Actuators A: Physical*, 1999, **74**, 52-55.
7. M. J. Rand and J. F. Roberts, Silicon Oxynitride Films from the NO-NH<sub>3</sub>-SiH<sub>4</sub> Reaction, *Journal of the Electrochemical Society*, 1973, **120**, 446.
8. J. Steffens, M. A. Fazio, D. Cavalcoli and B. Terheiden, Multi-characterization study of interface passivation quality of amorphous sub-stoichiometric silicon oxide and silicon oxynitride layers for photovoltaic applications, *Solar Energy Materials and Solar Cells*, 2018, **187**, 104-112.
9. G. Kovačević and B. Pivac, Reactions in silicon–nitrogen plasma, *Physical Chemistry Chemical Physics*, 2017, **19**, 3826-3836.
10. N. I. Fainer, A. G. Plekhanov, M. N. Khomyakov, E. A. Maksimovskiy and Y. M. Rumyantsev, The influence of the conditions of synthesis on the composition and mechanical properties of silicon oxycarbonitride nanocomposite films, *Protection of Metals and Physical Chemistry of Surfaces*, 2017, **53**, 253-260.
11. T. Otani and M. Hirata, High rate deposition of silicon nitride films by APCVD, *Thin Solid Films*, 2003, **442**, 44-47.
12. N. Bahlawane, K. Kohse-Höinghaus, P. A. Premkumar and D. Lenoble, Advances in the deposition chemistry of metal-containing thin films using gas phase processes, *Chemical Science*, 2012, **3**, 929-941.
13. V. Tomar, D. Patil and D. Gautam, Deposition and characterization of SiON films using HMDS for photonics applications, *Semiconductor Science and Technology*, 2006, **22**, 43.
14. A. M. Wrobel, A. Walkiewicz-Pietrzykowska and I. Blaszczyk-Lezak, Reactivity of organosilicon precursors in remote hydrogen microwave plasma chemical vapor deposition of silicon carbide and silicon carbonitride thin-film coatings, *Applied Organometallic Chemistry*, 2010, **24**, 201-207.
15. J. W. Smith, S. M. Seutter and R. S. Iyer, Thermal Chemical Vapor Deposition of Bis (Tertiary-Butylamino) Silane-based Silicon Nitride Thin Films: Equipment Design and Process Optimization, *Journal of the Electrochemical Society*, 2005, **152**, G316.
16. J. Gumpher, W. Bather, N. Mehta and D. Wedel, Characterization of low-temperature silicon nitride LPCVD from bis (tertiary-butylamino) silane and ammonia, *Journal of the Electrochemical Society*, 2004, **151**, G353.
17. H. M. Park, J. Y. Lee, K. Y. Jee, S.-I. Nakao and Y. T. Lee, Hydrocarbon separation properties of a CVD-deposited ceramic membrane under single gases and binary mixed gas, *Separation and Purification Technology*, 2021, **254**, 117642.

18. V. E. Vamvakas, R. Berjoan, S. Schamm, D. Davazoglou and C. Vahlas, Low pressure chemical vapor deposition of silicon oxynitride films using tetraethylorthosilicate, dichlorosilane and ammonia mixtures, *Le Journal de Physique IV*, 2001, **11**, Pr3-231-Pr233-238.
19. E. Halova, S. Alexandrova, A. Szekeres and M. Modreanu, LPCVD-silicon oxynitride films: interface properties, *Microelectronics Reliability*, 2005, **45**, 982-985.
20. B. Kaghouché, F. Mansour, C. Molliet, B. Rousset and P. Temple-Boyer, Investigation on optical and physico-chemical properties of LPCVD SiO<sub>x</sub>N<sub>y</sub> thin films, *The European Physical Journal Applied Physics*, 2014, **66**, 20301.
21. S. Alexandrov, A. Kovalgin and D. Krasovitskiy, A study of CVD of gallium nitride films by in situ gas-phase UV spectroscopy, *Le Journal de Physique IV*, 1995, **5**, C5-183-C185-190.
22. K. Kachel, D. Siche, S. Golka, P. Sennikov and M. Bickermann, FTIR exhaust gas analysis of GaN pseudo-halide vapor phase growth, *Materials Chemistry and Physics*, 2016, **177**, 12-18.
23. T. Ohba, T. Suzuki, H. Yagi, Y. Furumura and T. Hatano, Decomposition property of methylhydrazine with titanium nitridation at low temperature, *Journal of the Electrochemical Society*, 1995, **142**, 934.
24. M. M. Nolan, S. Y. Kim, A. Koley, T. Anderson and L. McElwee-White, In Situ Investigation of the Thermal Decomposition of Cl<sub>4</sub>(CH<sub>3</sub>CN)W(NiPr) During Simulated Chemical Vapor Deposition, *European Journal of Inorganic Chemistry*, 2019, **2019**, 3661-3666.
25. F. Lloret, K. J. Sankaran, J. Millan-Barba, D. Desta, R. Rouzbahani, P. Pobedinskas, et al., Improved Field Electron Emission Properties of Phosphorus and Nitrogen Co-Doped Nanocrystalline Diamond Films, *Nanomaterials*, 2020, **10**, 1024.
26. W. G. Zhang and K. J. Hüttinger, CVD of SiC from methyltrichlorosilane. Part II: Composition of the gas phase and the deposit, *Chemical Vapor Deposition*, 2001, **7**, 173-181.
27. J. Arnó, Z. Yuan and S. Murphy, Fourier Transform Infrared Characterization of Downstream Gas-Phase Species Generated by Tetraethylorthosilicate/Ozone Atmospheric Pressure Reactions, *Journal of the Electrochemical Society*, 1999, **146**, 276-280.
28. M. Yoshimoto, K. Takubo, M. Komoda and H. Matsunami, Gas phase reactions diagnosed by mass analysis in photo-assisted chemical vapor deposition of silicon nitride, *Applied Surface Science*, 1994, **79**, 264-269.
29. T. Sorita, T. Satake, H. Adachi, T. Ogata and K. Kobayashi, Mass Spectrometric and Kinetic Study of Low-Pressure Chemical Vapor Deposition of Si<sub>3</sub>N<sub>4</sub> Thin Films from SiH<sub>2</sub>Cl<sub>2</sub> and NH<sub>3</sub>, *Journal of the Electrochemical Society*, 1994, **141**, 3505.
30. N. I. Fainer, A. G. Plekhanov, A. N. Golubenko, Y. M. Rumyantsev, E. A. Maksimovskii and V. R. Shayapov, Structure and elemental composition of transparent nanocomposite silicon oxycarbonitride films, *Journal of Structural Chemistry*, 2017, **58**, 119-125.
31. H. Pedersen, Time as the Fourth Dimension: Opening up New Possibilities in Chemical Vapor Deposition, *Chemistry of Materials*, 2016, **28**, 691-699.
32. D. K. Russell, I. M. Davidson, A. M. Ellis, G. P. Mills, M. Pennington, I. M. Povey, et al., The kinetics and mechanism of the pyrolysis of manganese and manganese silicide CVD precursors, *Chemical Vapor Deposition*, 1998, **4**, 103-107.
33. K. C. Topka, G. A. Chliavoras, F. Senocq, H. Vergnes, D. Samelot, D. Sadowski, et al., Large temperature range model for the atmospheric pressure chemical vapor deposition of silicon dioxide films on thermosensitive substrates, *Chemical Engineering Research and Design*, 2020, **161**, 146-158.
34. M. D. Hanwell, D. E. Curtis, D. C. Lonie, T. Vandermeersch, E. Zurek and G. R. Hutchison, Avogadro: an advanced semantic chemical editor, visualization, and analysis platform, *Journal of Cheminformatics*, 2012, **4**, 17.

35. W. Knolle, L. Wennrich, S. Naumov, K. Czihal, L. Prager, D. Decker, et al., 222 nm Photo-induced radical reactions in silazanes. A combined laser photolysis, EPR, GC-MS and QC Study, *Physical Chemistry Chemical Physics*, 2010, **12**, 2380-2391.
36. R. Pandey, L. Patil, J. Bange, D. Patil, A. Mahajan, D. Patil, et al., Growth and characterization of SiON thin films by using thermal-CVD machine, *Optical Materials*, 2004, **25**, 1-7.
37. J. H. Lee, C. H. Jeong, J. T. Lim, V. A. Zavaleyev, S. J. Kyung and G. Y. Yeom, SiO<sub>x</sub>N<sub>y</sub> thin film deposited by plasma enhanced chemical vapor deposition at low temperature using HMDS–O<sub>2</sub>–NH<sub>3</sub>–Ar gas mixtures, *Surface and Coatings Technology*, 2007, **201**, 4957-4960.
38. R. González-Luna, M. Rodrigo, C. Jiménez and J. Martínez-Duart, Deposition of silicon oxinitride films from hexamethyldisilazane (HMDS) by PECVD, *Thin Solid Films*, 1998, **317**, 347-350.
39. V. Tomar, L. Patil and D. Gautam, Deposition and characterization of silicon nitride films using HMDS for photonics applications, *Journal of Optoelectronics and Advanced Materials*, 2008, **10**, 2657-2662.
40. B. Xia, M. L. Fisher, H. Stemper and A. Misra, One-step growth of HfSiON films, *Thin Solid Films*, 2008, **516**, 5460-5464.
41. Z. Tijanić, D. Ristić, M. Ivanda, I. Bogdanović-Radović, M. Marciuš, M. Ristić, et al., Low Temperature Deposition of SiN<sub>x</sub> Thin Films by the LPCVD Method, *Croatica Chemica Acta*, 2012, **85**, 97-100.
42. L. Gorla-Gatti, A. Iannone, A. Tomasi, G. Poli and E. Albano, In vitro and in vivo evidence for the formation of methyl radical from procarbazine: a spin-trapping study, *Carcinogenesis*, 1992, **13**, 799-805.
43. A. J. Carmichael, K. Makino and P. Riesz, Quantitative aspects of ESR and spin trapping of hydroxyl radicals and hydrogen atoms in gamma-irradiated aqueous solutions, *Radiation Research*, 1984, **100**, 222-234.
44. H. Chandra, I. M. Davidson and M. C. Symons, Unstable intermediates. Part 202. The use of spin traps to study trialkylsilyl and related radicals, *Journal of the Chemical Society, Perkin Transactions 2*, 1982, 1353-1356.
45. H. Chandra, I. M. T. Davidson and M. C. R. Symons, Use of spin traps in the study of silyl radicals in the gas phase, *Journal of the Chemical Society, Faraday Transactions 1: Physical Chemistry in Condensed Phases*, 1983, **79**, 2705-2711.
46. J. Pola, A. Galíková, A. Galík, V. Blechta, Z. Bastl, J. Šubrt, et al., UV Laser Photolysis of Disiloxanes for Chemical Vapor Deposition of Nano-Textured Silicones, *Chemistry of Materials*, 2002, **14**, 144-153.



Table of Contents text

Coupled analysis by GC-MS, ESR, NMR during CVD of  $\text{SiO}_x\text{N}_y$  implemented for the first time, highlighting reaction pathways. Silanamine precursor serves as dual source of Si and N, producing silylated radicals and at least fifteen gaseous by-products.

L. Decosterd, K. C. Topka, B. Diallo, D. Samelot, H. Vergnes, F. Senocq, B. Caussat, C. Vahlas, M.-J. Menu\*

**An innovative GC-MS, NMR and ESR combined, gas-phase investigation during chemical vapor deposition of silicon oxynitrides films from tris(dimethylsilyl)amine**

